Elastic and shear moduli of coal measure rocks derived from basic well logs using fractal statistics and radial basis functions

C. Özgen Karacan *

CDC/NIOSH, Pittsburgh Research Laboratory, Disaster Prevention and Response Branch, 626 Cochrans Mill Road, PO Box 18070, Pittsburgh, PA 15236, USA

A B S T R A C T

Gamma ray, density, sonic and core logs obtained from two boreholes drilled over a longwall panel in Southwestern (SW) Pennsylvania were analyzed for formation boundaries, log-derived porosities and densities and for rock elastic properties from sonic transit times. Gamma ray (GR) and density logs (DL) were analyzed using univariate statistical techniques and fractal statistics for similarity and ordering of the log data in depth. A Fourier transformation with low-pass filter was used as a noise elimination (filtering) technique from the original logs. Filtered data was tested using basic univariate and fractal statistics, rescaled range (R/S) and power spectrum (PS) analysis to compare the information characteristics of the filtered logs with the original data. The randomness of log data in depth was analyzed for fractional Gaussian noise (fGn) or fractional Brownian motion (fBm) character.

A new prediction technique using radial basis function (RBF) networks was developed to calculate shear and Young's moduli of the formations when sonic logs are not available. For this approach, the filtered logs were used as input to an RBF based upon a combination of supervised and unsupervised learning. The network was trained and tested using rock elastic properties calculated from the sonic log of one of the boreholes. The network was used to predict the elastic and shear moduli of the coal-measure rocks over a longwall coal mine in SW Pennsylvania. This approach demonstrated that it could be used for prediction of elastic and shear moduli of coal-measure rocks with reasonable accuracy.

1. Introduction

The properties of coal-measure rocks within the longwall overburden are important because of their controlling effect on fluid storage and flow before and after coal extraction. Methane inflow into the mines from fractured strata during longwall mining and production potential of the methane degasification boreholes drilled from surface (gob gas ventholes or GGVs) to capture these emissions are influenced by reservoir, elastic and strength characteristics of the overlying strata. Thus, the ability to accurately determine reservoir and elastic properties of the coal measure rocks is extremely important for ground control and methane control objectives in underground coal mining. The elastic modulus, or Young's modulus, and shear modulus are used when deformations in underground mines need to be computed. Experimentally, the elastic modulus can be determined from the stress–strain response of a rock sample subjected to uniaxial compression. However, this is a complicated and time consuming experiment.

With the advent of new computing and experimental techniques, complicated and time consuming experiments and methods to determine rock elastic and strength properties are being replaced by quicker, and may be even more accurate, techniques. For instance, the uniaxial unconfined compressive strength (UCS) test has been largely replaced by simpler, faster and cheaper "indirect" tests such as point loading method [1] and Schmidt hammer [2], although UCS was the main direct quantitative method for rock strength determination for many years. Triaxial testing of a core from a rock material to find rock elastic and strength properties is another difficult, expensive and complicated laboratory test, in which the stress state in the rock sample is axisymmetric and defined by the axial stress, confining pressure and pore pressure. The results of this test are usually studied in terms of Terzaghi's effective mean pressure and deviatoric stress which correspond to volume strain and the deviatoric strain [3].

In order to overcome the difficulties related to determination of elastic properties of rocks by laboratory tests, it has become very popular to develop alternatives that would predict the elastic moduli of rocks using theoretical and empirical approaches. In these approaches, elastic and shear moduli are either related to simple physical properties like total porosity or to other mechanical properties, indices, and even to mineral composition of rocks that are determined in the laboratory or documented in the

* Tel.: +1 412 386 4008; fax: +1 412 386 6595.
E-mail address: cok6@cdc.gov

literature. However, as shown by the equations and conversion factors in the literature, it is clear that there are no unique factors and relations which can be used, even for the same type of rock. Also, experimental data available in the literature that sometimes is used to generate predictive equations mainly concerns limestones and cemented sandstones. Poorly cemented sandstones are difficult to characterize due to coring and heterogeneity problems. Low permeability of shales and their sensitivity to water complicate the tests by showing a strong interaction of the strain rate and the saturating fluid. Thus, literature data on shales needs to be handled carefully [3] for generating conversion factors and relations.

Palchik [4] reported the relationships between Young's modulus (E) and σ_c are obtained from the stress–strain responses of six carbonate rocks (dolomites, chalks and limestones) collected from different locations in Israel. He reported that the use of these empirical equations is not universal, but rather limited, since empirical constants can only be used for the carbonate rocks with which the tests were conducted. In addition, he noted that although E generally increases with increasing σ_c, these relations have different degrees of reliability with R^2 ranging from 0.57 to 0.98. Thus, he proposed a stress–strain model based on Haldane's distribution function to predict the elastic modulus of intact carbonates. He concluded that this model is better correlated with the experimental data for Israeli carbonate rocks having a UCS <100 MPa.

Deriving the elastic properties of a rock from its mineralogical content has been a tempting alternative approach [3]. The idea behind this approach is that the mineralogical characteristics of rocks influence the macromechanical properties and especially the rock strength. Techniques such as variational methods [5] and the theory of homogenization [6] are available for this objective. However, these methods are far from practical and require powerful numerical procedures. Thus, approaches based on a restrained number of parameters accessible from drilling logs, which give reasonable estimations of rock mechanical properties, were sought.

Mineral composition, grain size and microstructure are known to be the most important parameters that influence rock strength and elastic properties. Bemer et al. [3] also stated that it is difficult to address sandstones since their composition is extremely variable and their elastic properties depend on the stress state due to their often nonlinear behavior. Sabatakikis et al. [7] conducted a large number of laboratory tests on intact marlstones, limestones and sandstones. Index properties such as porosity, unit weight, mineralogical content, Schmidt hammer and point loading indices, as well as the strength under uniaxial and triaxial compression were determined. From the analyses of the data, conversion factors relating rock strength to rock compositional properties and index properties were calculated. They reported that textural characteristics in limestones are more important than mineral composition for rock strength. In sandstones, the mineral composition was found to be more important.

Further attempts to determine UCS, shear and Young's moduli included data driven approaches. These used material properties to generalize the relations between input and output space for nonlinear approximations. Grima [8] used fuzzy modeling and artificial neural networks (ANN) for the modeling of unconfined compressive strength of rock samples. He compared results with those of statistical models and the empirical relationship of Verwaal and Mulder [9]. Density, porosity and equotip hardness test (EHT) values were used as the input parameters for his models. He reported that data driven models are more reliable than statistical and empirical models. Sonmez et al. [10] developed an artificial neural network-based chart which considers σ_c and unit weight as input to predict elastic modulus of intact rock. Maji and Sitharam [11], on the other hand, applied back propagation algorithm and radial basis function to predict elastic modulus of jointed rocks from the elastic modulus of intact rocks, confining pressure, joint frequency, joint inclination and joint roughness. They concluded that these models could accurately represent the effect of confining pressure and joint properties.

One of the major disadvantages inherent in all laboratory tests, and in the derived correlations is that the tested samples will not be in the in situ conditions anymore when they are tested in the laboratory. It is very difficult or nearly impossible to create exactly the same underground stress and fluid saturation conditions in the laboratory due to the many interacting parameters under in situ conditions. In addition, the scaling effect in the laboratory measurements due to sample size and the testing effects at the "end points" of the sample may be an issue to interpret the results. Furthermore, the elastic moduli can be either dynamic or static, and undrained or drained. Standard laboratory tests usually give access to static and drained elastic moduli, which can then be directly used to compute strains. However, dynamic undrained tests can be conducted either "in situ" or with complex and time consuming methods.

Geophysical well logs and seismic, such as time-lapse seismic, techniques can measure the in situ properties of rocks and fluid reservoirs. For instance, a well log interrogates the formations around the wellbore with different techniques and obtains response data as the tool travels downward or upward in a borehole. Among the well log techniques that are most frequently used by oil and gas companies are spontaneous potential (SP), gamma ray (GR), density log (DL) and sonic log (SL) that calculate basic formation properties such as porosity, density, shale content and boundaries of the formations of interest. Sonic logs that employ compression and shear waves to interrogate the formations can also be used as the source of data for an "in situ" geotechnical evaluation of the rock formations since acoustic travel time is explicitly tied to the density and the elasticity of the medium [12]. They also can give access to dynamic undrained elastic moduli, which require data on the compressibility of the saturating fluids to be turned into dynamic drained elastic moduli.

Gamma ray and density logs are two of the conventional logging techniques frequently employed by mining companies to determine formation boundaries, formation thicknesses and formation types. On the other hand, full wave sonic logs are seldom used since they are more expensive to run, data intensive and more complicated in terms of operation procedures. However, SL is capable of providing more detailed information about the condition of the borehole, surrounding strata, their elastic properties and how they may behave during underground mining. This information is particularly important for ground control and for effective control of methane from a fractured zone using gob gas ventholes (GGV).

The objective of this study is to develop a new technique to calculate shear and elastic (Young's) moduli of the formation, which can then be used to determine bulk modulus and Poisson's ratio, using radial basis function (RBF) networks. The method is based on processing of GR and DL by Fourier transform, fractal statistics and then modeling using RBF to predict elastic and shear moduli, when full wave sonic logs are not available or too costly to obtain. This approach evaluates the "in situ" rock elastic properties of coal-measure rocks and for prediction purposes with a reasonable accuracy.

2. Borehole data evaluated in this study

Data from two exploration boreholes (EBH-1 and EBH-2) were used in this study. These two boreholes were in the same mining

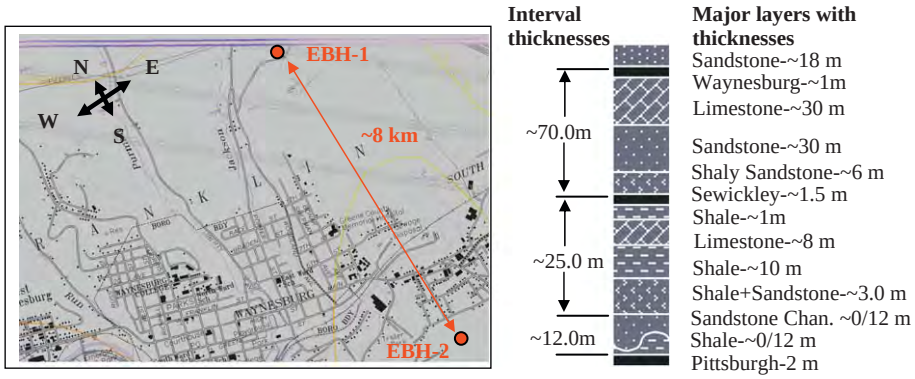

Fig. 1. Exploration boreholes (EBH) studied in this paper, their locations in the field and a generalized stratigraphic column of this area.

area but were ~8 km apart from each other and were located south and north of Waynesburg, Pennsylvania (Fig. 1).

EBH-1 and EBH-2 were drilled for exploration purposes to characterize the mine roof and the mining coal thickness at the two locations. They were drilled from surface to an approximate depth of 12.2 m with rotary techniques and continued with a 5.8 cm core drill until the bottom of the Pittsburgh coal bed was exceeded by about 6.1 m. Cores were fully recovered from EBH-1 and were marked for depths and lithology identification. The total depths of EBH-1 and EBH-2 were 255.1 and 263 m in depth, respectively. After completion of drilling, boreholes were logged with gamma and density tools for the entire length of the borehole. In addition, EBH-2 also was logged with a full wave sonic tool.

In this area of the Northern Appalachian basin, the overburden depths above Pittsburgh coal seam ranges between 152 and 274 m. A generalized stratigraphic section of the strata above the Pittsburgh coal bed in the study area is shown in Fig. 1. At some locations in this area, there is a sandstone paleo-channel complex and associated shale unit overlying the Pittsburgh seam.

The Sewickley coal bed and the rider coals (not shown in this figure) directly above the Pittsburgh coal bed are believed to be the primary sources of gob gas during longwall mining. Gas released from the Pittsburgh rider coals located in the caved zone is expected to migrate to the mine ventilation system, while gas from the Sewickley coalbed and from any other gas-bearing horizons above the caved zone migrates to the pressure sink of the operating gob gas ventholes in the fractured zone.

3. Characterization of coal-measure rocks using well logs

3.1. Characterization of rock formations using gamma ray and density logs

In this section, gamma ray and density logs obtained from EBH-1 and EBH-2 were evaluated with core logs to characterize the coal-measure rocks above Pittsburgh coal bed. Fig. 2 shows the lithological log, thicknesses of major layers defined from the driller's log, and raw gamma and density logs from EBH-2. At EBH-2, the top of the Pittsburgh coal bed was at a depth of 252 m. The general sequence between 204 and 241 m above the Pittsburgh seam layer can be divided in four sections (dotted lines in Fig. 2). These zones are mainly alternating sequences of limestone, shale, and sandstone, as determined from gamma ray and density logs. In each of these zones, thin shale layers (A, C–F) are sandwiched between stronger limestone or sandstone formations. In this log, the Sewickley coalbed is located at "B" (low gamma ray, low density) and overlain by carbonaceous shale (A) which records a high gamma ray reading accompanied by a decreased density.

Raw gamma ray and density logs, as well as lithological logs and strata thicknesses, for EBH-1 are shown in Fig. 3. At this location, the Pittsburgh coal bed is found at a depth of 254 m. Similar sequence of layers, as in EBH-2, is observed at this location too. Limestone layers are separated by shale layers as annotated on gamma and density logs (A–G). Some of the low density readings ($A^{/}$ and $B^{/}$) are associated with carbonaceous and limy shales and with highly porous shale units. At this borehole site, the Sewickley coal seam is thicker than it is at EBH-2 location. This might influence the amount of methane that will be experienced once this location is undermined. Also, this location is missing the thick Pittsburgh sandstone that overlays the Pittsburgh coal seam. The absence of this layer may affect the fracturing and the amount of methane associated with this layer.

3.2. Shale content and porosity of coal-measure formations at EBH-1 and EBH-2 using GR and DL

The GR log is a record of a formation's radioactivity. During deposition of coal measure shales, its clay constituents adsorb ions of the heavy radioactive elements from mineralized waters involved in the weathering process of igneous formations. Due to adsorption of radioactive elements, fine grained sediments such as clayey sands and shales are generally quite radioactive. On the other hand, carbonate rocks have low radioactivity since they are mainly derived from calcareous marine-life skeletal material. Similarly, pure sandstones have low radioactivity due to the well-ordered structure of quartz that exclude impurities during crystallization. Since sandstones are usually porous, they may be penetrated with radioactive ions and clays later [13].

The GR log is usually used to identify boundaries, primarily shale units from other low radioactivity formations, and to quantify shale volume of the rock formations. In fractured formations, an increase in the gamma ray reading without concurrently higher formation shaliness can be observed. This increase has been explained by deposition of uranium salts along the discontinuity surfaces of a fracture or within the crack itself. Also, it is not uncommon to find as much as 0.01% uranium or thorium in dark bituminous shale units, which increases the gamma ray reading [13].

In this study, formation type and thicknesses were first identified from the GR logs of the boreholes for calculating shale volume. The clean-formation readings for each rock type were determined by locating the clean sandstone and limestone units in the logging data. Pittsburgh sandstone and limestone intervals were suitable for this purpose since they were free from shales. The GR reading for coal was determined based on the average GR reading along Sewickley layer. For the shale GR reading, the average reading of the shale intervals was determined and used in

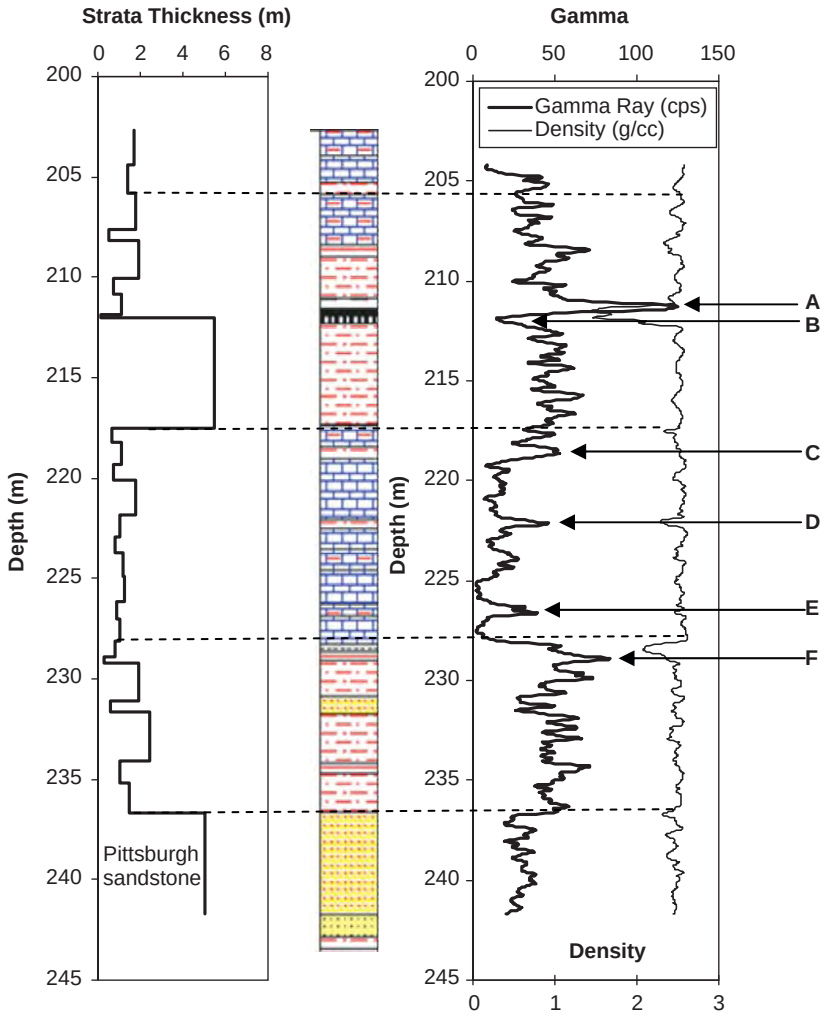

Fig. 2. Lithological log of EBH-2 with thicknesses of major layers defined from driller's log and raw gamma and density logs.

the calculations. In shale volume calculations, each interval was calculated separately using respective clean-formation readings. The aim was to minimize errors from using a single formation GR value for the entire borehole interval.

Porosities were calculated based on the readings of the density log which corresponds to bulk density. There are a variety of factors affecting bulk density measurements. One of the most important is the shaliness of the formation which affects the measurement by the amount of its contribution to the total signal. In this study, a correction was made by the volume of shale in order to obtain a shale-corrected density measurement [13].

The following equation can be used to quantify the shale volume by using GR log [14]:

$$V_{shale} = \frac{GR_l - GR_{clean\ rock}}{GR_{shale} - GR_{clean\ rock}} \quad (1)$$

In this equation, GR_l is the gamma ray reading (cps, count per second) from the log. The other two terms are the GR readings of the clean formations (clean sandstone and limestone) and the pure shale [13,14]. These readings were obtained from the formations and using the methodology mentioned in the previous paragraph.

Bulk density (ρ_b), on the other hand, is determined from density log, from which porosity can be calculated (Eqs. (2) and (3)). However, before porosity can be determined, the lithology of the formation, the matrix density, and the fluid density filling the pore space must be known. For a clean formation of known matrix density, ρ_{ma}, with a fluid of average density, ρ_f, the linear sum of the contributions can be used to calculate porosity (ϕ) as described in Karacan [15] and by using below equations:

$$\rho_b = \phi\rho_f + (1-\phi)\rho_{ma} \quad (2)$$

$$\rho_b = \rho_{b_{sh,free}}(1 - V_{shale}) + \rho_{shale}V_{shale} \quad (3)$$

Fig. 4 shows the shale content and porosity values for EBH-1. The calculations show that the lowest shale percentage is found in limestone bearing units at depths of 225.5 m, 230.1–234.7 m, with an average shale amount of 5–10%. Within this interval, there are layers of weak shale formations at 229.9 and 233.5 m. These and similar layers are potentially weak interfaces to be affected by mining stresses and by the resultant bedding plane separations. Outside of limestone intervals, the average shale content in the strata varies from 40% to 50%.

Fig. 4 also shows the porosity values calculated in the EBH-1 borehole using the density log. This plot shows that porosity values are generally low (0–0.1), except for some intervals where values exceeding 0.5 are observed. These locations are at 210.3 m (A), 217.9 m (B), 224.0–225.5 m (C–D), 233.1 m (E), 237.8 m (F) and 243.8 m (G), where 224 m corresponds to the Sewickley coal bed. These intervals are generally associated with fractures, laminated layers and shales inter-layered between limestone units. These high porosity intervals can result in weak spots in the strata leading to eventual fracturing and separation, which may also

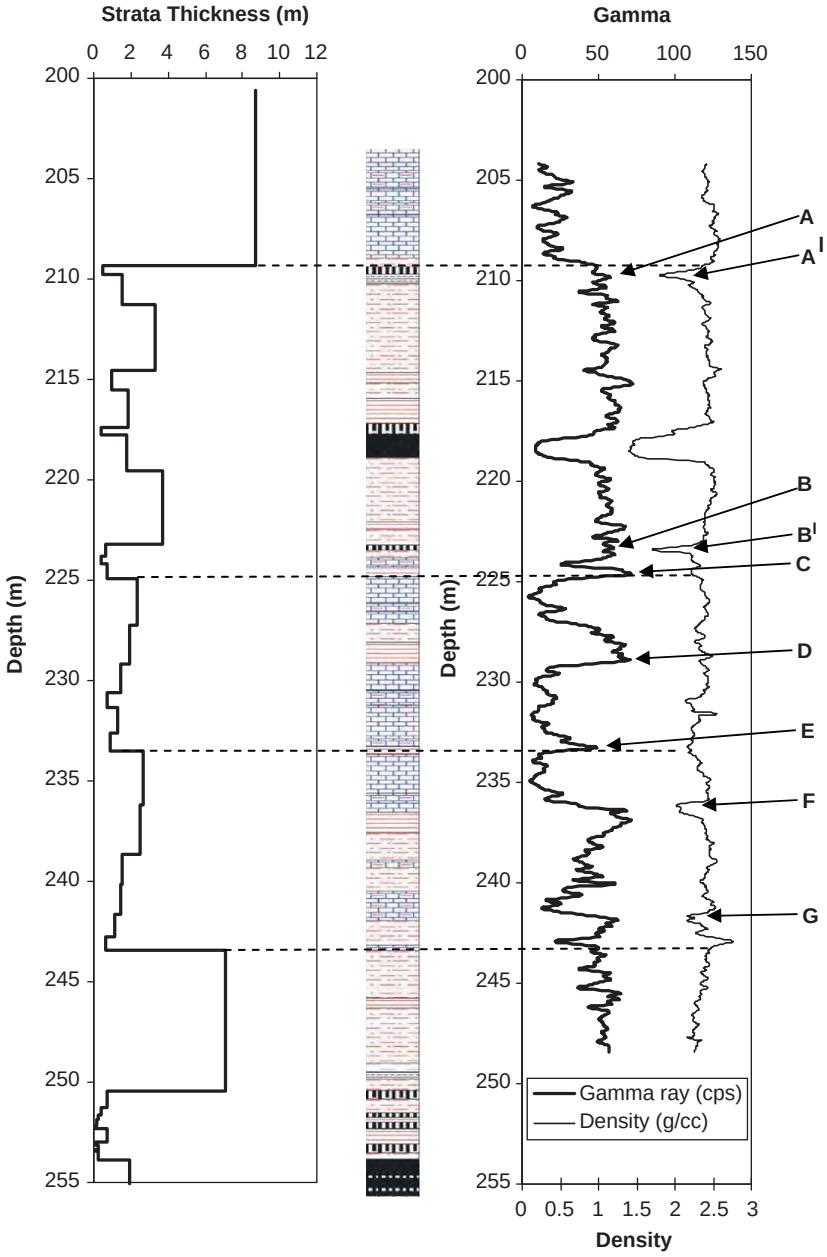

Fig. 3. Raw GR, DL, lithological log and strata thicknesses for EBH-1.

promote methane flow towards any borehole or to the mine. These areas may potentially be the reservoirs of free methane that will flow into a pressure sink once the fracture connection is established during mining.

Similar observations can also be made for EBH-2 location based on shale content and porosity calculations, which are shown in Fig. 5. In this borehole, average shale content in the sandy-shale layers is around 30–40%. Higher shale-content areas are interbedded with more competent limestone sequences and the Pittsburgh sandstone 217.9–228.6 m and below 236.2 m, respectively. The layer that is almost exclusively shale at around 211.8 m is closely associated with thin carbonaceous shale and is either a clay-filled fracture or a fracture surface that is carrying a high amount of radioactive ions.

The calculated porosities for EBH-2, based on the density log, are also shown in Fig. 5. The values indicate that most porosity values are around 0.1. However, there are higher porosity sections based on the strata intervals. The highest values are marked from A to H on the figure and they are generally associated with shale layers, especially where clay content is high and possibly where some natural fractures within the strata or along the bedding interfaces are present. In these sections, porosities were as high as 0.4–0.5 and in some instances even more. These high porosities can be related to weak spots in the strata that may lead to fracturing and bedding plane separation. They can also constitute pockets for free methane and can serve as flow paths within the formation.

3.3. Shear modulus and Young's modulus calculation at EBH-2 using sonic log

In sonic logging, ultrasonic frequencies are employed in the form of compressional and shear waves. Compressional wave measurement used in sonic logging exhibits longitudinal particle motion and can be propagated in solids, liquids and gases. The

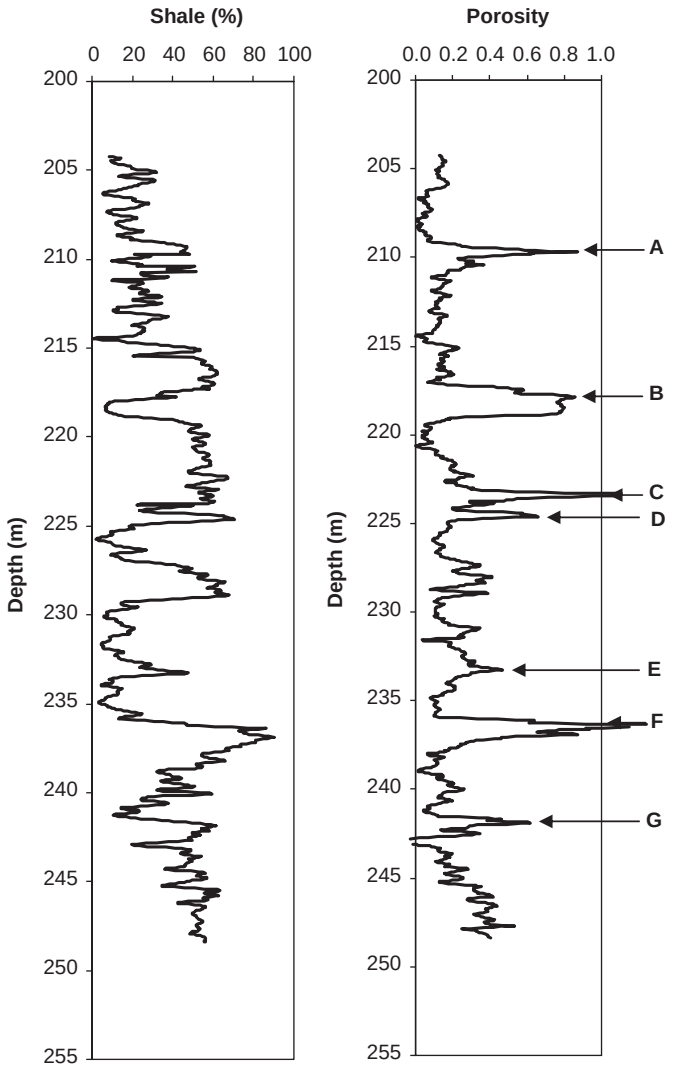

Fig. 4. Shale content and porosity log calculated from raw gamma and density logs obtained from EBH-1.

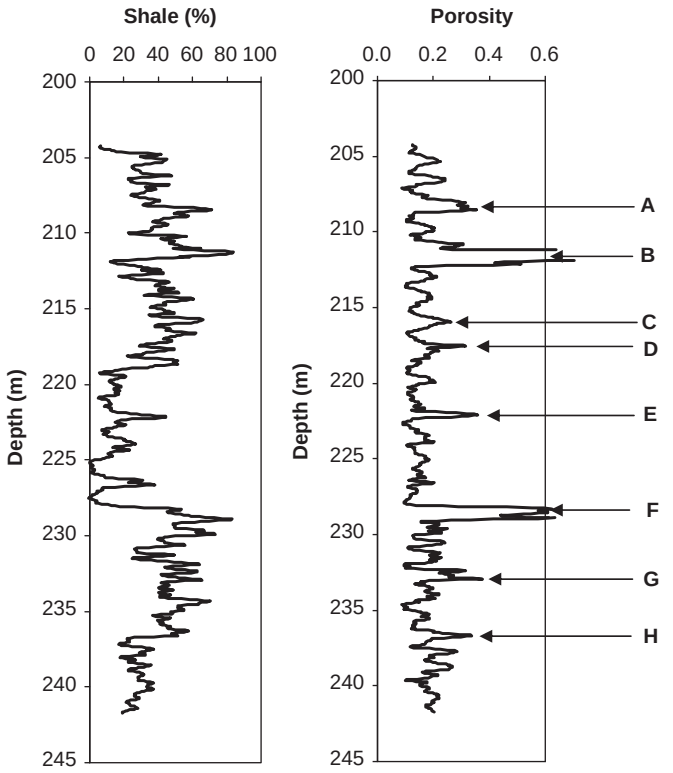

Fig. 5. Shale content and porosity log(s) calculated from raw gamma and density logs obtained from EBH-2.

shear wave, on the other hand, is a transverse wave, in which the direction of propagation is perpendicular to the direction of particle displacement. In case of a compressional wave, the acoustic wave alternately compresses the surrounding medium on a forward movement and rarifies it on a backward movement [13].

Velocities obtained from sonic logs can be used as the fundamental information for rock classification and geotechnical evaluation. Acoustic travel time of any type of ultrasonic disturbance is explicitly tied to the density and the elasticity of the medium. Compressional waves are characterized by first arrival times. Although slower than compressional waves (0.5–0.7 times), shear waves are usually stronger and can be identified in the total wave train.

In this paper, shear modulus and Young's modulus values were calculated using the velocities of compressional and shear waves determined from full wave sonic logs as described in [12]. Dynamic moduli were calculated using both compressional and shear waves and a determination of dynamic Poisson's ratio (n) using Eqs. (4)–(6):

$$G = \rho V_s^2 \tag{4}$$

$$v = \left\{ \left(\frac{V_p}{V_s}\right)^2 - 2 \right\} \Big/ \left\{ 2\left(\frac{V_p}{V_s}\right)^2 - 2 \right\} \tag{5}$$

where ρ is the density, G is shear modulus, V_p and V_s are the compressional and the shear wave velocities, respectively. The Young's modulus (E) and the bulk modulus (K) can then be calculated using

$$E = 2G(1 + v) \tag{6}$$

$$K = \frac{E}{3(1 - 2v)} \tag{7}$$

Young's moduli and shear moduli for EBH-2 are given in Fig. 6. This figure shows that highest Young's and shear moduli are associated with limestone and competent sandstone layers. The values in these layers are as high as 4 and 9 GPa for shear modulus and Young's modulus, respectively. When the layer is shale, sandy or limy shale, or coal, values decrease abruptly to values as low as 1–2 GPa, indicating weaker rock units that will be deformed easily when subjected to high stress and strain conditions prevailing during mining. These weak layers and their interfaces with stronger rocks are candidates for fracturing and bedding plane separations to form increased permeability pathways for methane migration into longwall gobs.

Despite the crucial information obtained that is related to possible rock behavior under certain stress and strain conditions, sonic logging is more unconventional than both density and gamma ray logging, especially in mining-related strata characterization. Part of the reason why it is not used as often as the other two is the cost and time associated with recording and processing sonic data. Processing sonic full wave profiles can also be a tedious task since the arrival times of compressional and shear waves should be determined from an entire wave train to calculate Young's modulus, shear modulus and sonic porosity.

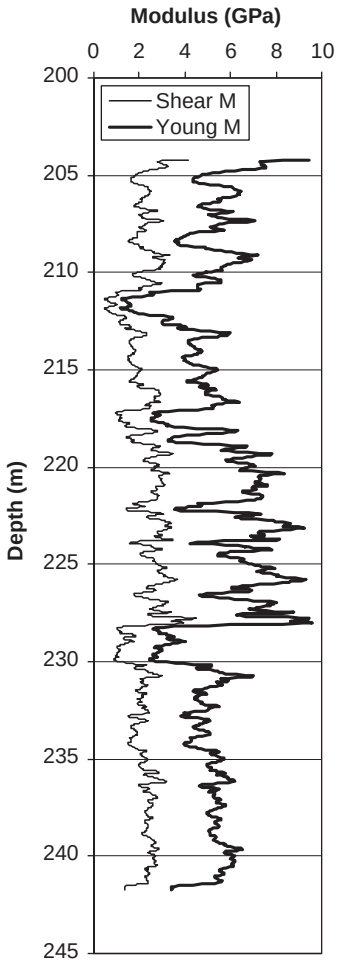

Fig. 6. Shear and Young's moduli of the formations calculated based on compression and shear-wave sonic velocities at EBH-2 drill site.

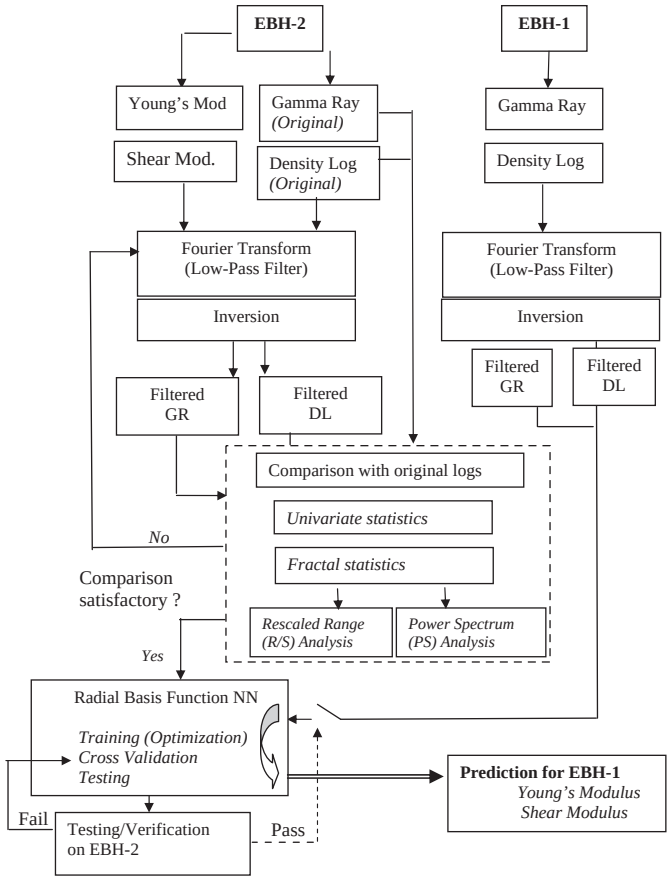

Fig. 7. A flowchart representation of the details of the mathematical methodology followed for the log-data analysis and generation of radial basis function network.

4. Methodology development for log-data treatment and for generating rock elastic properties from gamma and density logs

The aim of this section is to gain a better understanding of the data ordering in available logs from EBH-1 and EBM-2 using rescaled range (R/S) and power spectrum (PS) analyses to determine their fractal (fGn/fBm) character. This information is used to compare the original logs with the filtered ones generated using Fourier transform (FT) to make sure that both sets of data carry the same or similar information content and data ordering. Next, a methodology to generate shear and Young's moduli using filtered gamma and density records is developed. The method is based on using filtered GR and DL with radial basis function networks to predict available Young's and shear moduli in the same borehole. An optimized network system is then used to predict the elastic and shear moduli for EBH-1 using its gamma and density readings, which unfortunately did not have a sonic log record.

The flowchart in Fig. 7 graphically presents the details of the methodology followed for this approach. The details of the techniques will be given in the next sections and in the appendices in this paper.

4.1. Stationarity of self-affine fractal character of log traces

In analyzing the self-affine fractal data sequences and the ordering of data within, stationarity and ergodicity are important characteristics to be determined. A stationary data ensemble is one whose ensemble average properties are independent of depth or time. Thus, if the logs show an increasing (or decreasing) trend with depth, even if the ensemble averages are the same, the ensemble is non-stationary and, therefore, it is also non-ergodic [16,17]. These two properties usually determine which mathematical techniques, fractional Gaussian noise (fGn) or fractional Brownian motion (fBm), are appropriate for an analysis.

Fractional Gaussian noise and fractional Brownian motion are data sequences with self-affine fractal character that can be used to describe time series and geological distributions as well as heterogeneities. Self-affine fractal sequences are statistical in character and mathematically described by using "Hurst coefficient", which is a dimensionless number between 0 and 1 and represents the intermittency of the data. Unlike pure Gaussian (white noise, or uncorrelated data), fGn exhibits spatial correlation between data points. fBm is the integral of fGn and contains more low frequency components than high frequencies. The characteristics of fGn and fBm are mathematically described in Appendices A and B.

Histograms of fGn- and fBm-type data sequences present differences, too. Histogram of fGn is Gaussian where the histogram of fBm is box-shaped, or rectangular. In this study Gaussians, which represented the data distributions with accuracies of 0.94 and 0.96, were fitted to those data in the depth interval of interest (204.2–240.8 m) and a good representation of histograms with these curves were observed. The Gaussian shape of the histograms suggested that the data series could be classified as fGn. Also, DL and GR of EBH-2 (Fig. 2) were locally increasing or decreasing based on the formations within this interval. However, there was not a consistent trend in GR and DL

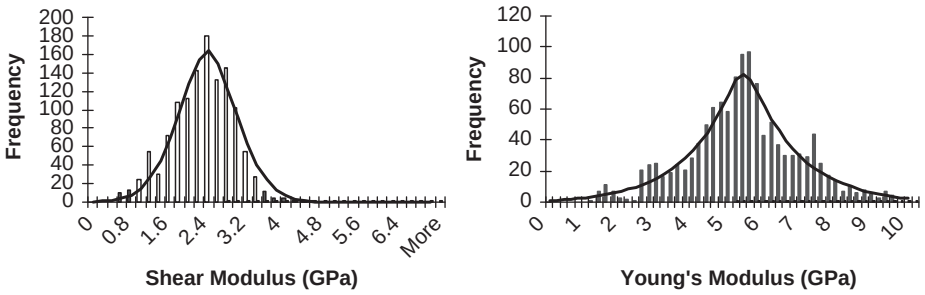

Fig. 8. Histogram for shear and Young moduli data calculated from SL of EBH-2 and their Gaussian representation.

within this interval, suggesting that both curves are stationary. A similar stationarity property could be proposed for Young's and shear moduli by examining the sonic-log derived data shown in Fig. 6. They both could be represented almost perfectly by Gaussian distribution with an accuracy of 0.98 (Fig. 8).

4.2. Noise reduction in log data (EBH-2) by Fourier transforms method

Random noise (RN) can greatly affect the result of certain types of analyses by shifting the location of the peak, which leads to systematic overestimation of the height of the peak and to amplification after differentiation. RN can also decrease the prediction capability of any predictive methods by creating additional nonlinearities and local minimums that may distort the approach to convergence in iterative techniques. Since random noise is distributed over all frequencies and the real signal is typically limited to low frequencies, a reduction of high frequency components improves the signal/noise (S/N) ratio. Before proceeding further in the elastic and shear moduli generation using GR and DL in RBF, the original logs were filtered to remove the high frequency signals, which correspond to possible noise. The purpose of this step is to increase S/N and thus improve the prediction capability of RBF on the true "signal".

There are different methods available to generate a smoother data trace. For instance, a smoother log signal can be generated from the original curve by averaging every "*n*" values of the curve and plotting these averages at the middle of each of the averaged intervals. However, this process significantly reduces the number of data points, and thus the information content. Running average is another option but it creates large lags at the ends of the data sequence.

For filtering the data sequence, the aim is to generate a curve with improved S/N that honors the properties of the original curve and that is statistically similar. This can be done by generating a curve with the same (or close) mean, standard deviation, the same average values and self-affine fractal properties investigated by different methods as the original curve. In this work, the objective of "non-destructive" filtering on well logs was achieved by employing a low-pass filter using Fourier transform methods. Well logs are processed as discrete and finite signals and transformed into frequencies for filtering of high-frequency signals, while trying to preserve as much of the original information content as possible.

During FT, selected parts of the frequency spectrum "G" can easily be subjected to piecewise mathematical manipulations based on the frequency of the signal. These manipulations result in a modified or "filtered" spectrum. Therefore, signal smoothing can be performed by completely removing higher frequency components while information-bearing low frequency components are retained. By eliminating undesirable high-frequency components, we can filter a data array to remove noise and other artifacts. Taking an inverse Fourier transform converts the data back into the depth domain [16]:

$$g_j = \frac{\Delta\omega}{2\pi} \sum_{m=1}^{N} G_m e^{2\pi i(j-1)(m-1)/N} \tag{8}$$

where ω is the angular frequency of a sine or cosine function, and $f = \omega/2\pi$.

Fig. 9 compares the original GR and DL of EBH-2 with the curve generated by averaging the data every 0.61 m and with the filtered curve generated using the low-pass filter in Fourier transform methods. This figure shows that the filtered curve better represents the original curve in both cases without destroying the overall information in high and low frequency regions.

The success of FT filtering techniques is further investigated by comparing the descriptive statistics of the original log data with the filtered one to see if similar mean, standard deviation and median can be captured. The Hurst exponents and global scaling parameters obtained from the two sets to characterize the fractal nature of the original and filtered data using rescaled range and power spectrum were also studied in the following sections.

4.3. Univariate measures to investigate the statistical similarity of filtered and original logs of EBH-2

The filtered logs were investigated using univariate and fractal statistics to see if they honored the properties of the original curves. Comparing the histograms obtained from filtered GR and DL logs to the original histograms showed that FT preserved the Gaussian properties of the original logs with accuracies of 0.93 and 0.98 for GR and DL, respectively. A similar filtering and comparative study for shear and Young's moduli logs were also performed and proved that these data could also be filtered without affecting the character of the original moduli curves.

In addition to Gaussian checks of original and filtered log data, statistical parameters of original and filtered sequences of GR, DL, shear modulus and Young's modulus from EBH-2 were compared. This approach checked if the filtered data sequences honored the basic statistical features of the original data sequence. Table 1 shows the results of these analyses. Values of mean, standard error, median and standard deviation are very similar for the original and filtered logs of EBH-2. These results encourage the use of filtered data instead of noisier, original data in the subsequent analysis and proxy model development for prediction of elastic properties of rock strata for EBH-2 and EBH-1.

4.4. Self-affine fractal analysis on logs of EBH-2: power spectrum and rescaled range analysis for determining Hurst (Hu) and global scaling (H) coefficients

Univariate statistical analyses on the original and filtered sequences of different logs obtained from EBH-2 show statistical

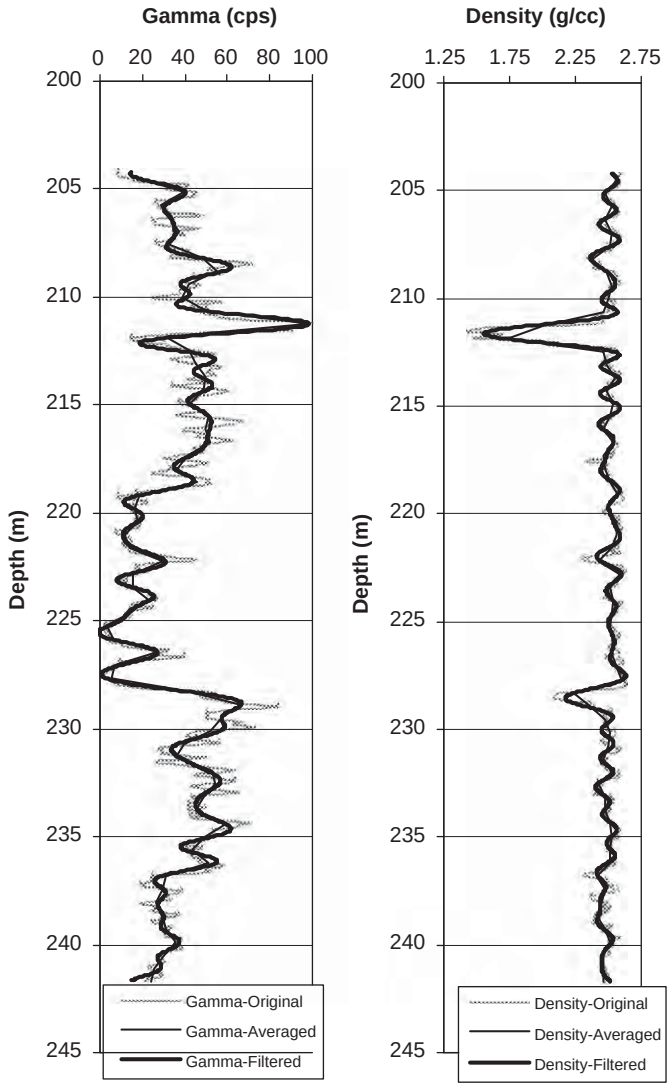

Fig. 9. Comparison the original GR and DL of EBH-2 with the curve generated by averaging the data in every 0.61 m and with the filtered curve generated using Fourier transform methods.

similarities between data sequences before and after FT. In order to have a better understanding of the data ordering in specific geophysical logs, multivariate measures, such as rescaled range analysis and power spectrum analysis should be used (Appendices C and D).

Fractional Gaussian noise-type data can be analyzed by Hurst coefficients (Hu), which can be evaluated numerically by rescaled range analysis. R/S is considered a robust method for investigating the presence of correlations in random events. This analysis is a measure of how a sequence varies as the distance (lag) between data points increases according to $R/S = (\alpha N)^{Hu}$, where N is the lag and α is a constant. In general, the longer the interval studied (the lag), the greater the rescaled range. In R/S analysis, the *logarithm of rescaled range* is plotted against the *logarithm of lag*. If the resulting plot gives a straight line for the region of long lags, the slope of this line is denoted as "*Hu*". The values of *Hu* determined from *R/S* are given in Table 2.

Fig. 10 shows the R/S plots for original and filtered sequences for GR and DL from EBH-2. These plots show that filtering changes the behavior of R/S in the whole lag range. However, *Hu* at long lags is not severely affected. The *Hu* values calculated for original and filtered data using these graphs ranged between 0.2 and 0.4

Table 1
Basic univariate statistical parameters of original and filtered sequences of GR (A), DL (B), shear modulus (C) and Young modulus (D) logs from EBH-2.

	Original	Filtered
(A) GR (cps)		
Mean	36.242	36.262
Standard error	0.534	0.495
Median	36.690	35.935
Standard deviation	18.744	17.234
(B) DL (g/cc)		
Mean	2.473	2.473
Standard error	0.004	0.004
Median	2.500	2.499
Standard deviation	0.147	0.138
(C) Shear modulus (GPa)		
Mean	2.213	2.213
Standard error	0.018	0.016
Median	2.260	2.279
Standard deviation	0.631	0.558
(D) Young modulus (GPa)		
Mean	5.318	5.319
Standard error	0.043	0.040
Median	5.330	5.284
Standard deviation	1.529	1.411

Table 2
Results of *R/S* analysis for original and filtered data series of GR, DL, shear modulus and Young's modulus (EBH-2).

	Hu (from original log)	Hu (from filtered log)
R/S on EBH-2 logs		
Gamma	0.420	0.405
Density	0.299	0.285
Shear moduli	0.401	0.447
Young's moduli	0.248	0.285

for density and gamma logs (Table 2). These values are in $0 < Hu < 0.5$ range and represent anti-persistent nature of the logs.

The *Hu* values were also calculated for shear and Young's moduli logs (Table 2) for their original and filtered values from EBH-2. Comparing *Hu* values of these logs with the corresponding values of DL and GR shows that the *Hu* values are close to each other for shear modulus-GR and Young's modulus-DL pairs. This indicates, in the physical sense, that shear modulus is mostly related to the clay or shale content in a formation and thus to gamma ray readings, whereas the elastic modulus of a formation is more related to its bulk density.

Power spectrum analysis is the next technique to be used in investigating the fractal character and ordering of the data sequence. Power spectral density is a statistical measure based on the Fourier transform of the original discrete sequence (e.g. a well log). In this analysis, the *logarithm of the square of amplitude array* (spectral density) is plotted against the *logarithm of angular frequency*. The resulting early slope is denoted as β (spectrum power), which is related to global scaling coefficient, H, by $\beta_{fGn} = \leftarrow -(2H_{fGn} - 1)$ for fGn-type series. These values are given in Table 3 for GR and DL of EBH-2.

Spectrum power and global scaling coefficients (H) calculated using the PS approach are given in Table 3. The table shows that the global scaling coefficient, H_{fGn}, which is allowed to change between +1 and −1, is somewhat larger than *Hu* obtained from *R/S* analysis. However, they are close to the values of unfiltered "original" log data and these and the fractal dimensions still show a pairing between GR-shear modulus and Young's modulus-DL.

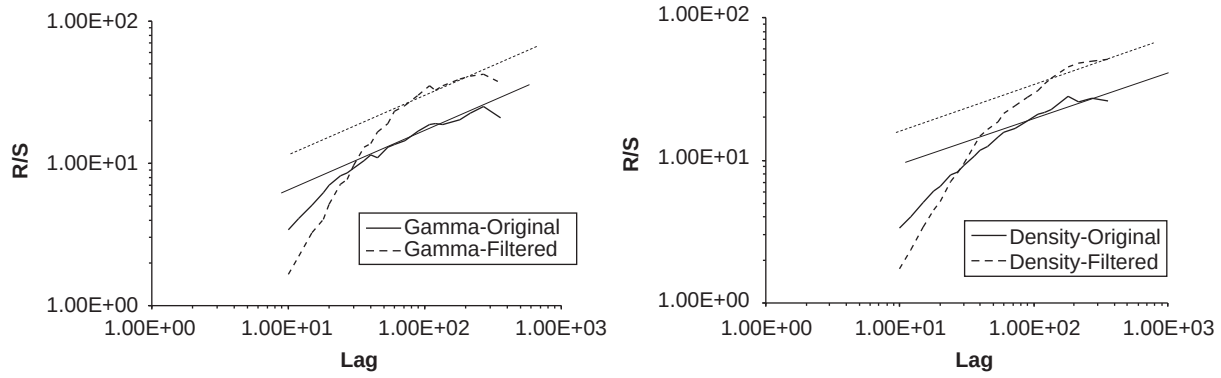

Fig. 10. *R*/*S* plots for original and filtered sequences for GR and DL from EBH-2. The straight lines are the best linear fits to the long-lag regions of the data series.

Table 3
Results of power spectrum (PS) analysis for original and filtered data series of GR, DL, shear modulus and Young's modulus (EBH-2).

	β_{fGn} (original)	H_{fGn} (original)	β_{fGn} (filtered)	H_{fGn} (filtered)
PS analysis on EBH-2 logs				
Gamma	−0.126	0.563	−0.125	0.562
Density	−0.525	0.763	−0.724	0.862
Shear moduli	−0.240	0.620	−0.150	0.575
Young's moduli	−0.517	0.759	−0.654	0.827

Fig. 11 shows the power spectrum of the filtered GR and DL data of EBH-2. Since the power spectrum is obtained via Fourier transform, the power spectrum of filtered (Fourier transformed) data is related to the power spectrum of the original sequence by the convolution theorem [16]. This results in a power spectrum plot of filtered function versus frequency that is constant up to some frequency value, $\tilde{f}$. This value is the "roll-off frequency," which is the value at which a filter adds a constant to within some percentage to the spectral density of the original sequence from $-\infty$ to $\tilde{f}$. Above $\tilde{f}$, the amount added rapidly decreases [16].

The results presented in this section show similarities between the univariate and fractal statistical measures of the original and filtered data. In other words, the filtering technique applied to the original data honors the properties of the original data sequence without critical distortions.

5. Development of a radial basis function network for prediction of Young and shear moduli from gamma and density logs

A neural network simulates a highly interconnected, parallel computational structure of the brain with many relatively simple individual processing elements, called *neurons* [18] to approximate nonlinear or complex data. Neurons are networked (topology) in a number of ways depending on problem type and complexity. Within the hidden layer, the inputs are summed and processed by a nonlinear function, called a transfer function or axon. The nonlinear nature of the function plays an important role in the performance of a neural network.

The process of finding a suitable set of weights for the network is called network optimization or "training". The most common way of training the networks is via supervised training algorithms, which require repeated showings (epochs) of both input vectors and the expected outputs of the training set to the network to allow it to learn the relations. However, in some specific cases (Kohonen self-organizing maps, radial basis functions), unsupervised networks are also used with success.

The neural network computes its output at each epoch and compares it with the expected output (*target*) of each input vector in order to calculate the error. An error is defined for a given pattern (input–output) and summed over all output neurons over the entire epoch. The error is summed over all neurons to give an average mean squared error (MSE) [18]. Minimizing this error is the goal of the training process. During error minimization, it is preferable to find the global optimum rather than the local optimum. Once the training phase is complete, the performance of the network needs to be validated on an independent data set. Cross validation is a model evaluation method that indicates the performance of the ANN when it is confronted with data it has not yet seen. It is important that validation data not be used as part of training. More detail is found in [19,20].

One of the most widely used topologies is the feed forward (FF) network because it can be applied in almost every kind of modeling, general classification, and regression. Radial basis function is the most widely used network after FF. The key to successful implementation of these networks is to find suitable centers for the Gaussian functions. Radial basis functions are typically used to build up function approximations of the form

$$y(x) = \sum_{i=1}^{N} w_i \phi(\|x - c_i\|) \leftarrow \tag{9}$$

where the approximating function $y(x)$ is represented as a sum of N radial basis functions, each associated with a different center c_i, and weighted by an appropriate coefficient w_i. In this equation, ϕ is the radial basis function. Approximation schemes of this kind have been particularly used in time series prediction and in control of nonlinear systems exhibiting sufficiently simple chaotic behavior.

The sum (Eq. (9)) can also be interpreted as a rather simple single-layer type of artificial neural network called a radial basis function network, with the radial basis functions taking on the role of the activation functions of the network. It can be shown that any continuous function on a compact interval can in principle be interpolated with arbitrary accuracy by a sum of this form if a sufficiently large number, N, of radial basis functions is used. Radial basis function networks have a static Gaussian function as the nonlinearity for the hidden layer processing elements. One of the most commonly used types of radial basis functions is Gaussian function:

$$\phi(r) = e^{-\beta r^2}, \quad \beta > 0 \tag{10}$$

The Gaussian function responds only to a small region of the input space where the Gaussian is centered. Suitable centers can be found using either supervised or unsupervised learning

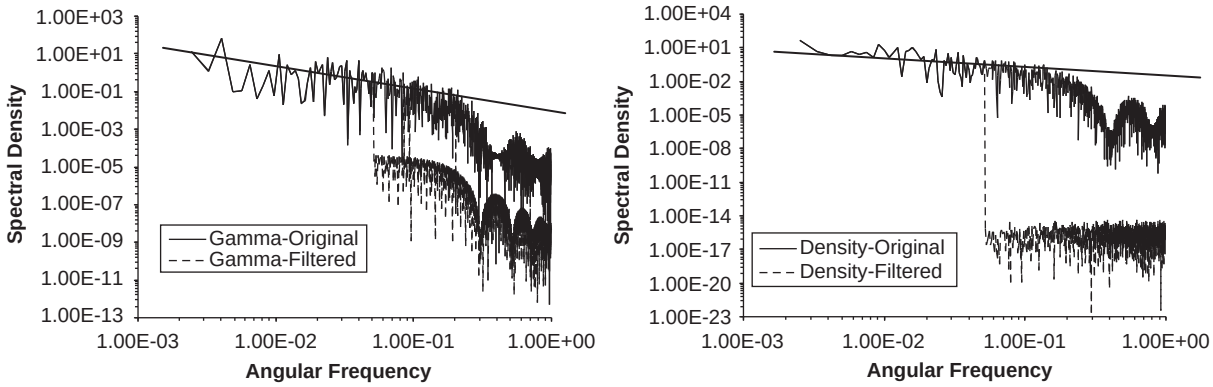

Fig. 11. Power spectrum plots of original and filtered GR and DL (EBH-2). The straight solid lines are the linear fits to the short-lag regions of the data series. Plots also show the frequency roll-off when applying FT to filtered data prior to PS analysis.

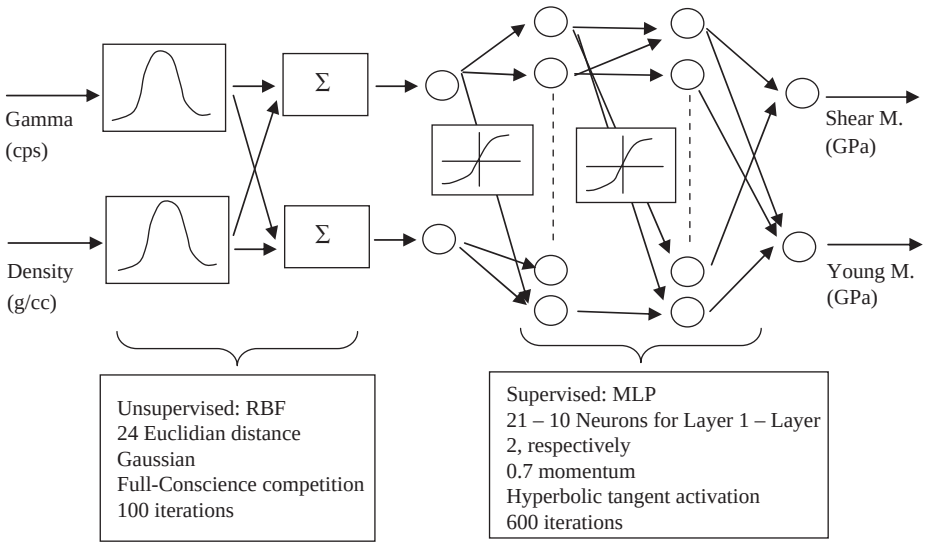

Fig. 12. Architecture of RBF-MLP network developed to calculate shear and Young's moduli from GR and DL readings.

approaches, the latter which may in some cases produce better results. In order to take advantage of both learning methods, a hybrid supervised-unsupervised topology was applied in this study to build the RBFs.

In this approach, the simulation started with the training of an unsupervised layer. This layer was trained based on "Full-Conscience" competition. Its function derives the Gaussian centers and the widths from the input data. These centers are encoded within the weights of the unsupervised layer using competitive learning. During unsupervised learning, the widths of the Gaussians are computed based on the centers of their neighbors. The output of this layer is derived from the input data weighted by a Gaussian mixture [21]. By using the "Full-Conscience" algorithm in this process, the winning rate of each neuron is tracked and the weights are adjusted so that there will not be a single neuron dominating in the whole process but, rather, each neuron will have a chance in the learning process. At the conclusion of training, each neuron's weight represents reference data, which is later used for classification.

Once the unsupervised layer has completed its training, the supervised segment then sets the centers of Gaussian functions (based on the weights of the unsupervised layer) and determines the width (standard deviation) of each Gaussian. A 2-layer multilayer perceptron (MLP) was used for processing the weighted input at this stage.

For developing an RBF-based network, filtered GR and DL data were used as inputs instead of the original data, since they included less noise and were capable of representing the original logs. An RBF network having Gaussian inner functions and trained on a full-conscience unsupervised learning algorithm was used and the output was fed into a 2-step multilayer perceptron-based network, which was trained using a back-propagation algorithm. The graphical representation of the network and its major elements and parameters are shown in Fig. 12.

5.1. Optimization of the network

In optimization or training of the RBF network, filtered log data from GR, DL, shear and Young's moduli from EBH-2 were used. Each of these logs had 1231 evenly spaced data points. First, these data were randomized to eliminate the biases. Of the randomized input series (1231 log data points), 180 were tagged for cross validation, 180 were tagged for testing of the network response and the rest were allocated for training purposes. In optimization of the network, it was trained six times in such a way that the 180 optimization inputs were shifted in every training step within the whole training set in order to change the order of the inputs and thus to minimize the error caused by ordering of the data in the randomized set.

Table 4
Performance of network in testing phase for the prediction of shear and Young's moduli.

Performance measure	Shear-modulus	Young-modulus
MSE	0.0894	0.2906
Nominal MSE	0.3089	0.1592
Mean abs error (GPa)	0.2209	0.4213
Min abs error (GPa)	0.0001	0.0100
Max abs error (GPa)	1.0228	2.0058
R	0.8337	0.9183

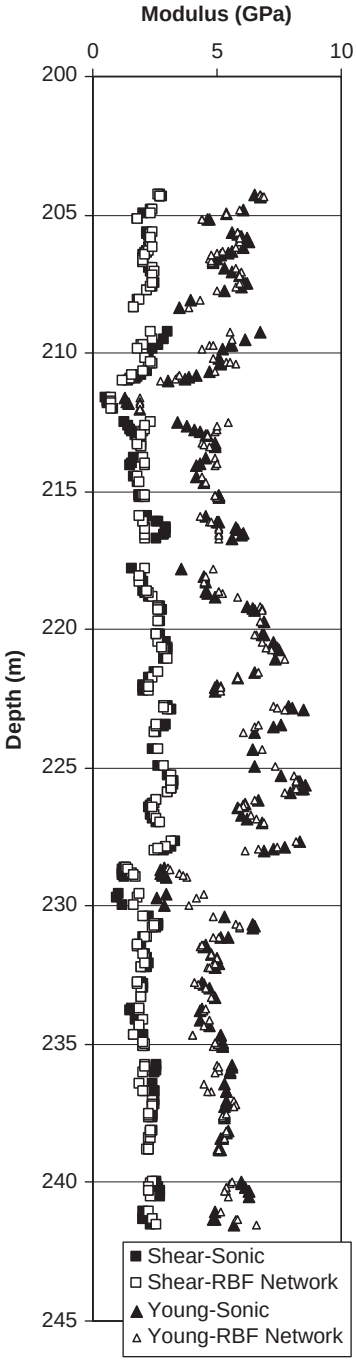

Fig. 13. Values calculated from sonic log and the predicted values based on gamma and density logs in EBH-2.

The optimization and the testing of the network were completed with mean squared errors of 0.015 for the optimization stage, and 0.089 and 0.290 for the testing stage when predicting shear and Young's moduli, respectively. The results showed that the expected and predicted values were close to each other indicating that the network achieved a reasonable predictive performance. The performance indicators of the testing phase are given in Table 4.

The moduli data used in the testing phase of the network (calculated from sonic log) and the RBF predicted values based on GR and DL are also plotted as a function of depth (Fig. 13). This graph shows that the modulus values calculated from the sonic log are in good agreement with the modulus values predicted by the network using gamma and density logs, encouraging its use as a predictive tool in other wellbores where gamma and density logs are present but sonic log is not available.

5.2. Application of RBF network for predicting shear and Young's moduli for EBH-1 and EBH-2 boreholes

The verification of the network was performed independently from the network optimization and testing protocol presented in the previous section. For this process, the arithmetic averages of GR and DL values within different stratigraphic intervals shown in Fig. 2 were calculated. Shear and Young's moduli values were also calculated using the same method of averaging. To test and verify the network response on this set of data, the average GR and DL values were given to the network as inputs and shear and Young's

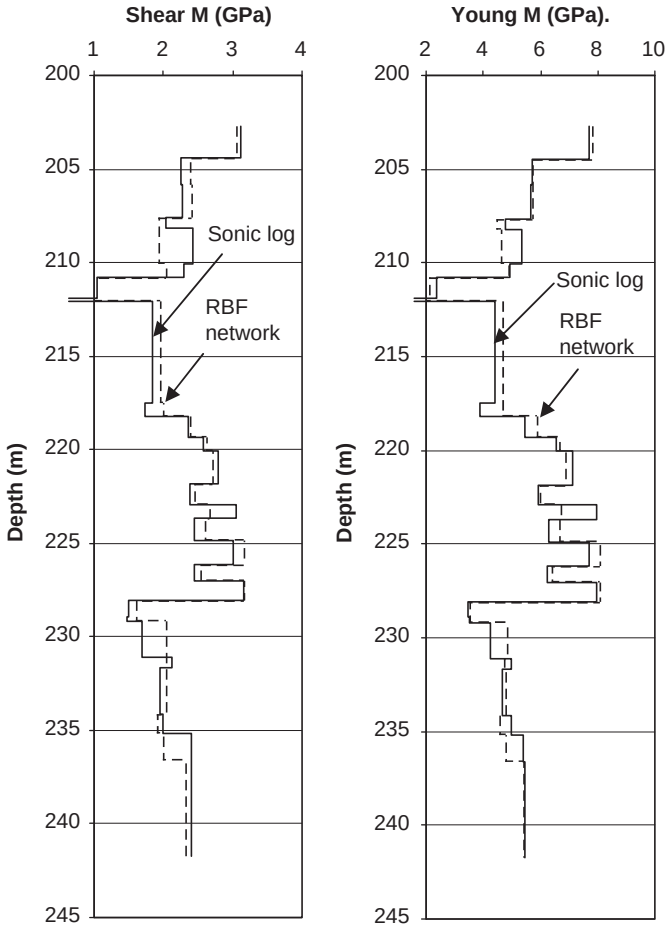

Fig. 14. Sonic-log derived shear and Young moduli versus network predictions using gamma and density logs (EBH-2).

moduli were predicted as outputs. The data from this prediction process data shown in Fig. 14. The network produced reasonable results for both moduli parameters with an accuracy of 0.92.

For further verification, the bulk modulus and Poisson's ratio calculated using sonic velocities were averaged within different stratigraphic intervals as described in the previous paragraph, and plotted against the bulk modulus and Poisson's ratio calculated using Young's and shear moduli from RBF output in Eqs. (6) and (7) as input (Fig. 15). The comparison shows that errors associated with RBF calculation of Young's and shear moduli are not amplified and bulk modulus and Poisson's ratio can also be calculated with a reasonable accuracy.

By using a similar technique, the GR and DL from EBH-1, for which a sonic log was not available, were averaged within the rock intervals. These average values were given to the network as inputs to predict shear and Young's moduli. The results of the network are presented in Fig. 16.

6. Summary and concluding remarks

In this study, GR, DL and sonic log data from two exploration boreholes from a mining area were analyzed for formation boundaries, shale contents, in situ porosity measurements and for rock elastic properties.

An analysis algorithm to process available log data was developed. According to this procedure, univariate statistical techniques and fractal statistics were used to study similarity and ordering of the log data in the depth scale. For this procedure, the data was smoothed using a Fourier transformation with a low-pass filter. Filtered data was tested using basic statistics and evaluated with rescaled range and power spectrum analyses to see if this data represented the information characteristics of the original data set.

Based on the fractal characteristics of the original and filtered data sequences, filtered data were used in a new prediction technique for shear and elastic moduli from DR and DL using radial basis function networks. This technique accurately predicted shear and elastic moduli, showing that it can calculate shear and Young moduli of the formations when sonic logs are either not available or too costly to obtain.

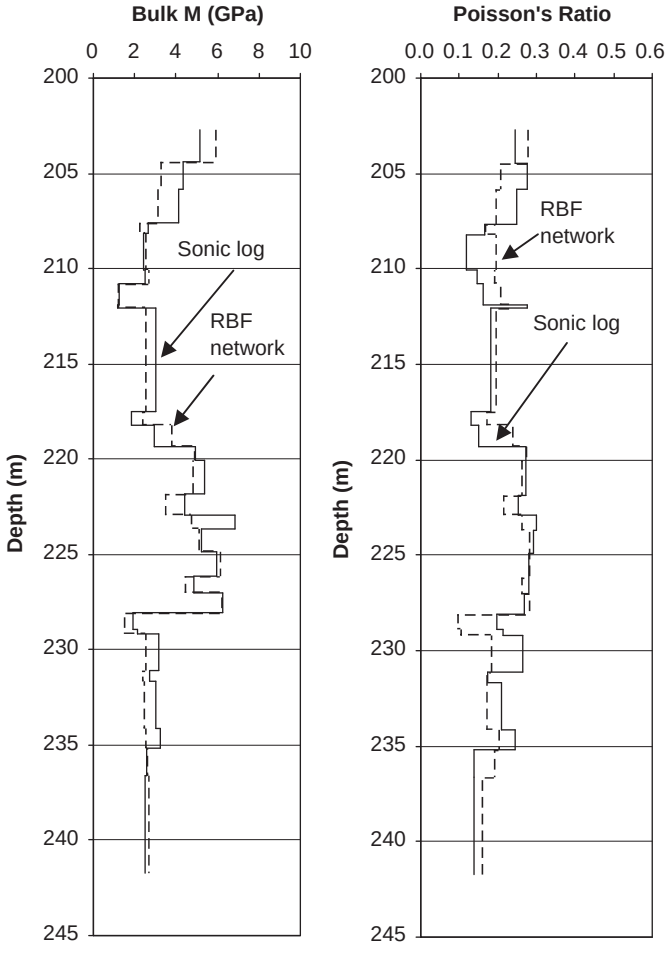

Fig. 15. Sonic-velocity derived bulk modulus and Poisson's ratio versus calculated ones (Eqs. (6)–(7)) using network-predicted Young and shear moduli from gamma and density logs (EBH-2).

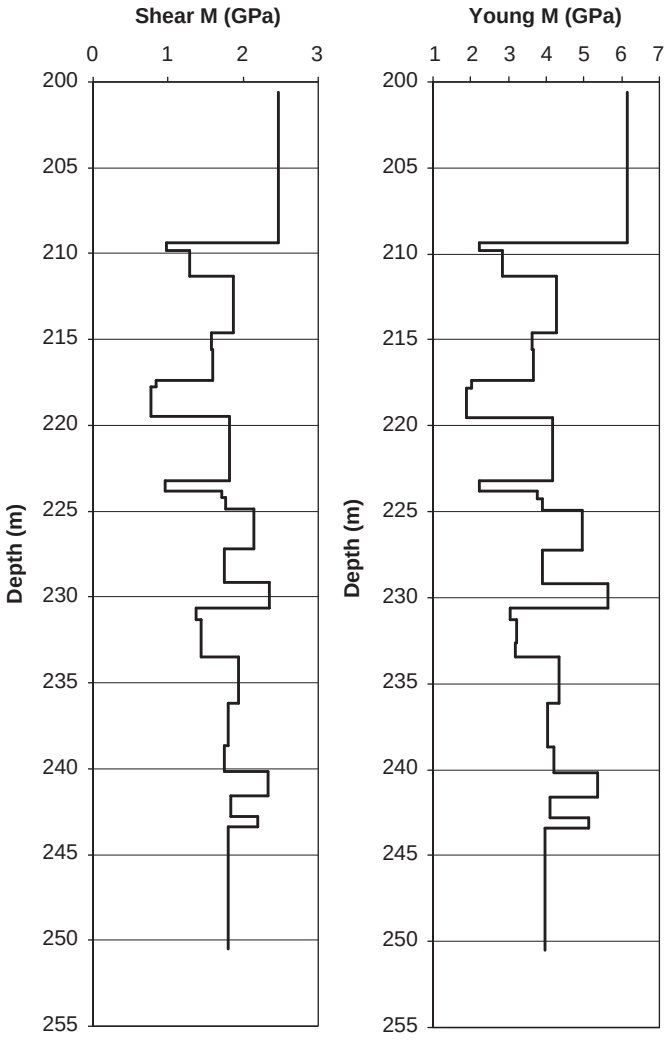

Fig. 16. Predicted average shear and Young's moduli for each strata sections in EBH-1 (Fig. 3) using the RBF network.

Appendix A. Fractional Brownian motion

Fractional Brownian motion is a non-stationary self-affine random process, defined by Mandelbrot and Van Ness [22] as

$$B_{Hu}(t) = \frac{1}{\Gamma(Hu+0.5)}\left[\int_{-\infty}^{0}\{|t-l|^{Hu-0.5}-|l|^{Hu-0.5}\}\,dB(l) + \int_{0}^{t}|t-l|^{Hu-0.5}\,dB(l)\right] \quad (A.1)$$

where $\Gamma(x)$ is the gamma function, and $B_{Hu}(t)$ an ordinary Gaussian process with zero mean and unit variance.

In this integral, the parameter Hu is the Hurst coefficient ($0<Hu<1$). When Hu is 0.5, the repeated integral produces uncorrelated noise (white noise). The sequence with $0.5<Hu<1.0$ is a persistent sequence. In other words, if the trend is increasing, an increasing trend can be expected in the future. If $0<Hu<0.5$, then the process is anti-persistent in nature [23,24].

Appendix B. Fractional Gaussian noise

Fractional Gaussian noises are family of random processes with stationary and Gaussian properties and long statistical dependence [25,26]. The fGn is more varied than fBm since it is fBm's derivative, which can be defined by

$$Z(x)=\lim_{\delta\to 0}\frac{B_{Hu}(x+\delta)-B_{Hu}(x)}{\delta} \tag{B.1}$$

It has zero mean and its variance is

$$Var\left\{\frac{B_{Hu}(x+\delta)-B_{Hu}(x)}{\delta}\right\}=V_{Hu}\delta^{2Hu-2} \tag{B.2}$$

where V_{Hu} is

$$\Gamma(1-2Hu)\frac{\cos(\pi Hu)}{\pi Hu} \tag{B.3}$$

Appendix C. Rescaled range analysis

Hurst coefficient can be evaluated numerically by rescaled range analysis (R/S analysis), which is a measure of how a sequence varies as the distance (lag) between data points increase. This measure has been initially observed and implemented for records of natural data in time. In this analysis, first, the natural records are transformed into a new variable, $X(t, N)$, the so-called accumulated departure of the natural record in time in a given year t ($t=1,2,\ldots,N$), from the average, $\bar{x}(t)$, over a period of N years. The transformation formula is

$$X(t,N)=\sum_{i=1}^{t}(x_i-\bar{x}_N)=\sum_{i=1}^{t}x_i-t\bar{x}_N \tag{C.1}$$

The rescaled range R/S, the range can be defined as $R(N)=\max_{1\leqslant t\leqslant N}N(t,N)-\min_{1\leqslant t\leqslant N}N(t,N)$, and the standard deviation by

$$S(N)=\frac{1}{N}\sum_{t=1}^{N}[x_t-\bar{x}_N]^2\Bigg)^{1/2} \tag{C.2}$$

by dividing the range with its standard deviation, many natural phenomena can be studied using this power relationship [27,28].

$$R/S=(\alpha N)^{Hu} \tag{C.3}$$

where Hu is the Hurst coefficient. In general, the longer the interval studied (the lag), the greater the rescaled range. In R/S analysis, the logarithm of rescaled range is plotted against the logarithm of lag. If the resulting plot gives a straight line for the region of *long lags*, the slope of this line is denoted as H.

R/S is considered as a robust method for investigating the presence of correlations in random events, or even if the data obey Gaussian statistics or not [28]. However, some authors suggest that spectral density technique should be applied first to confirm fBm and R/S should be applied later to some incremental series of the data [26].

Appendix D. Power spectrum and spectral density analysis

The spectral density is a statistical measure based on the Fourier transform of the original data. All of the information in a discrete sequence created by Fourier transform is retained in amplitude and phase, which can be converted back to the same sequence by inverse transform. The square of the amplitude array is called the "spectral density". In spectral density analysis, one should plot logarithm of spectral density against logarithm of frequency. The resulting early slope is denoted as β (spectrum power), which is related to global scaling coefficient, H, by

$$\beta_{fGn}=-(2H_{fGn}-1)\leftarrow\text{for fractional Gaussian noise, } fGn \tag{D.1}$$

and

$$\beta_{fBm}=-(2H_{fBm}+1)\leftarrow\text{for fractional Brownian motion, } fBm \tag{D.2}$$

For fGn, β (spectrum power) is between +1 and −1, inclusive. For fBm, β is between −1 and −3, exclusive. Also, $\beta_{fGn}\cong\beta_{fBm}-2$ [26].

References

[1] Broch E, Franklin JA. The point-load strength test. Int J Rock Mech Min Sci 1972;9:669–97.
[2] Schmidt E. A non-destructive concrete tester. Concrete 1951;59:51–4.
[3] Bemer E, Vincke O, Longuemare P. Geomechanical log deduced from porosity and mineralogical content. Oil Gas Sci Tech (Rev IFP) 2004;59:405–26.
[4] Palchik V. Use of stress–strain model based on Haldane's distribution function for prediction of elastic modulus. Int J Rock Mech Min Sci 2006;44:514–24.
[5] Watt P, Davies GF, O'Connell RJ. The elastic properties of composites material. Rev Geophys Space Phys 1976;14:541–63.
[6] Sanchez-Palencia E. Non-homogeneous media and vibration theory. Berlin: Springer; 1980.
[7] Sabatakis N, Koukis G, Tsiambos G, Papanakli S. Index properties and strength variation controlled by microstructure for sedimentary rocks. Eng Geol 2008;97:80–90.
[8] Grima MA. Neuro-fuzzy modeling in engineering geology. Rotterdam: Balkema; 2000.
[9] Verwaal W, Mulder A. Estimating rock strength with the equotip hardness tester. Int J Rock Mech Min Sci Geomech Abstr 1993;30:659–62.
[10] Sonmez H, Gokceoglu C, Nefeslioglu A, Kayabasi A. Estimation of rock modulus: for intact rocks with an artificial neural network and for rock masses with a new empirical equation. Int J Rock Mech Min Sci 2006;43:224–35.
[11] Maji VB, Sitharam TG. Prediction of elastic modulus of jointed rock mass using artificial neural networks. Geotech Geolog Eng 2008;26:443–52.
[12] Takahashi T, Takeuchi T, Sassa K. ISRM suggested methods for borehole geophysics in rock engineering. Int J Rock Mech Min Sci 2006;43:337–68.
[13] Dresser Atlas. Log review I. Dresser Atlas Division, Dresser Industries, 1974.
[14] Schlumberger. Log interpretation principles/applications. Schlumberger Wireline and Testing, Sugarland, Texas, 1991.
[15] Karacan CÖ. Reservoir rock properties of coal measure strata of the Lower Monongahela Group, Greene County (Southwestern Pennsylvania), from methane control and production perspectives. Int J Coal Geol 2009;78:47–64.
[16] Hardy HH, Beier RA. Fractals in reservoir engineering. Singapore: World Scientific Publication; 1994.
[17] Yeten B, Gumrah F. The use of geostatistics and artificial neural networks for carbonate reservoir characterization. Transp Porous Media 2000;41:173–95.
[18] Eberhart RC, Dobbins RW. Neural network PC tools: a practical guide. San Diego: Academic Press; 1990.
[19] Maier HR, Dandy GC. Neural networks for the prediction and forecasting of water resources variables: a review of modeling issues and applications. Environ Modelling Software 2000;15:101–24.
[20] Karacan CÖ. Modeling and prediction of ventilation methane emissions of US longwall mines using supervised artificial neural networks. Int J Coal Geol 2008;73:371–87.
[21] NeuroDimension. NeuroSolutions v. 5.0. Gainesville, FL, 2006.
[22] Mandelbrot BB, Van Ness JW. Fractional Brownian motions, fractional noises and applications. SIAM Rev 1968;10:422–37.
[23] Arizabalo RD, Oleschko K, Korvin G, Ronquillo G, Pardo E. Fractal and cumulative trace analysis of wireline logs from a well in a naturally fractured limestone reservoir in the Gulf of Mexico. Geofís Int 2004;43(3):467–73.

[24] Pan S-Y, Hsieh B-Z, Lu M-T, Lin Z-S. Identification of stratigraphic formation interfaces using wavelet and Fourier transforms. Comput Geosci 2008;34:77–92.
[25] Zeybek AD, Onur M. Conditioning fractal (fBm/fGn) porosity and permeability fields to multiwell pressure data. Math Geol 2003;35:577–603.
[26] Li F-C. Rescaled-range and power spectrum analysis on well logging data. Geophys J Int 2003;153:201–12.
[27] Chamoli A, Bansal AR, Dimri VP. Wavelet and rescaled range approach for the Hurst coefficient for short and long time series. Comput Geosci 2007;33:83–93.
[28] Pallikari F, Boller E. A rescaled range analysis of random events. J Sci Explor 1999;13:25–40.